

# CVT-Bench: Counterfactual Viewpoint Transformations Reveal Unstable Spatial Representations in Multimodal LLMs\*

Shanmukha Vellamcheti, Uday Kiran Kothapalli, Disharee Bhowmick, and Sathyanarayanan N. Aakur

CSSE Department, Auburn University, Auburn AL 36849, USA  
{szv0080,uzk0006,dzb0110,san0028}@auburn.edu

**Abstract.** Multimodal large language models (MLLMs) achieve strong performance on single-view spatial reasoning tasks, yet it remains unclear whether they maintain stable spatial state representations under counterfactual viewpoint changes. We introduce a controlled diagnostic benchmark that evaluates relational consistency under hypothetical camera orbit transformations without re-rendering images. Across 100 synthetic scenes and 6,000 relational queries, we measure viewpoint consistency, 360° cycle agreement, and relational stability over sequential transformations. Despite high single-view accuracy, state-of-the-art MLLMs exhibit systematic degradation under counterfactual viewpoint changes, with frequent violations of cycle consistency and rapid decay in relational stability. We further evaluate multiple input representations, visual input, textual bounding boxes, and structured scene graphs, and show that increasing representational structure improves stability. Our results suggest that single-view spatial accuracy overestimates the robustness of induced spatial representations and that representation structure plays a critical role in counterfactual spatial reasoning.

**Keywords:** Spatial reasoning · Multimodal LLMs · Long context visual reasoning

## 1 Introduction

Spatial understanding in modern vision and multimodal systems is typically evaluated by their ability to describe relationships between objects in a scene [18, 19]. Given an image, models are asked to identify objects and characterize spatial relationships such as left of, behind, or next to [21]. This formulation assesses whether models can interpret spatial structure from a fixed viewpoint. However, effective spatial reasoning often requires reasoning about how those relationships would appear from a different viewpoint. For example, consider a tabletop scene, shown in Figure 1, containing a gray cylinder, a yellow sphere, and a blue cube arranged in a row. A human agent standing on one side of the table observes

---

\* Project page: <https://shanmukha-here.github.io/CVT-Bench/>

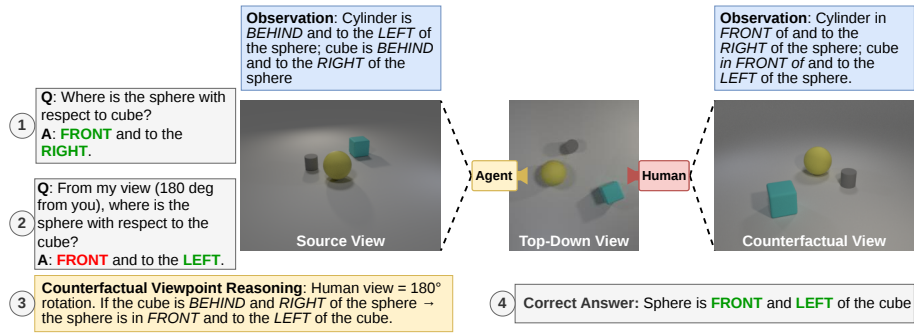


**Fig. 1: Counterfactual Viewpoint Reasoning.** An agent observes spatial relations from a single viewpoint (left). When queried from a human located  $180^\circ$  away, the model must transform these relations under the viewpoint change rather than reuse the original description. Although the sphere is front-right of the cube from the agent’s view, from the human’s viewpoint it becomes front-left. CVT-Bench evaluates whether multimodal models can perform such viewpoint-conditioned spatial reasoning reliably.

that the cylinder is in front of and to the right of the sphere and the cube in front of and to the left of the sphere. An assistive agent standing across the table, facing the same objects from the opposite direction, would perceive the spatial relationships differently: from its viewpoint, the cylinder is behind and to the left of the sphere and the cube is behind and to the right of the sphere. In a collaborative setting, if the human asks, “Hand me the cube to the left of the yellow sphere,” the assistant must reason about the scene from the human’s perspective rather than its own, using the yellow sphere as a relational reference. This requires not only recognizing spatial relationships from the current observation, but also inferring how those relationships would transform under a hypothetical change in viewpoint. This ability, commonly referred to as visual perspective taking [28, 38], reflects the capacity to maintain and transform an internal representation of spatial relationships under counterfactual motion.

Multimodal large language models (MLLMs) [12, 29, 36, 43] have shown strong performance on visual question answering [3, 18, 44], object grounding [41, 47], and spatial reasoning tasks [21], accurately identifying objects and describing their spatial relationships from visual input. Their success has motivated integration into embodied and decision-making systems such as robotics [14, 24] and autonomous driving [9, 10, 39], where spatial reasoning is essential for interaction and control. Most existing evaluations, however, are episodic, assessing reasoning within a single scene and fixed viewpoint. As a result, it remains unclear whether these models maintain spatial representations that support consistent reasoning under counterfactual viewpoint changes or across extended interactions involving multiple scenes. In realistic settings, agents must maintain spatial state over time, infer how relationships transform under hypothetical observer motion, and preserve relational consistency despite intervening observations. Evaluating these capabilities provides insight into whether multimodal models possess persistent

	Episodic F1 (BS=1)	Long-Ctx F1 (BS≥10)	Rotation Resilience	Text Benefit	SG Benefit	Tracking (BS=1)	Tracking (BS≥10)	Consistency (BS=1)	Consistency (BS≥10)	Context Stability
Gemini 3.1 Pro	✓	~	~	~	✗	✓	✓	✓	✓	✗
Kimi K2.5	~	✗	✗	~	✓	~	✗	✓	✗	✗
Qwen 3.5 Plus	✓	✗	~	✓	✗	✓	✗	✓	~	✗
Qwen 3.5 OS	✓	✗	✗	✓	~	✓	✗	✓	~	✗
GPT-5.2	✓	✓	~	✓	✗	✓	✓	✓	✓	✓

**Fig. 2:** High-level performance overview across ten diagnostic dimensions: episodic F1, long-context F1, rotation resilience ( $\Delta$  F1 between original and rotated views), text benefit ( $\Delta$  Text–Image F1), scene graph benefit ( $\Delta$  SG–Text F1), episodic and sequential spatial relation tracking, relational consistency ( $0^\circ$ – $360^\circ$  match rate), and context stability ( $\Delta$  F1 between episodic and sequential evaluation). Each cell displays a colored indicator: ✓ (strong), ~ (moderate), or ✗ (weak). GPT-5.2 uses BS=10.

spatial representations or rely primarily on view-dependent reasoning tied to individual observations.

To study this question, we introduce CVT-Bench, a diagnostic benchmark for evaluating spatial reasoning under counterfactual viewpoint transformations and sequential interaction. CVT-Bench presents scenes containing multiple objects and evaluates models’ ability to infer spatial relationships both from the observed viewpoint and under hypothetical camera rotations, without additional visual input. This setup isolates whether models can transform spatial relationships using an internal scene representation rather than relying solely on view-specific cues. Beyond episodic evaluation, CVT-Bench includes a sequential protocol in which models must maintain and update spatial state across multiple scenes within a continuous context, enabling analysis of reasoning stability under extended interaction. We introduce a new *spatial survival* metric that quantifies how long correct spatial relationships persist as interaction depth increases. This enables direct measurement of spatial reasoning stability over extended contexts. We further evaluate spatial reasoning across multiple input representations, including raw images, structured text descriptions, and graph-based scene representations, to examine how representation structure affects reasoning reliability. Our experiments (summarized in Figure 2) show that while multimodal models perform well in episodic settings, their accuracy drops under counterfactual viewpoint transformations and extended sequential contexts, revealing instability in maintaining spatial state. Structured representations significantly improve consistency, suggesting that representation structure plays a key role in enabling reliable perspective-conditioned spatial reasoning.

In this work, we make the following **contributions**: (1) we introduce CVT-Bench, a benchmark for evaluating counterfactual viewpoint reasoning and visual perspective taking in multimodal large language models; (2) we propose a unified protocol that distinguishes between episodic and sequential spatial reasoning, en-

abling controlled analysis of spatial state maintenance over extended context; (3) we introduce a representation-controlled evaluation across visual, textual, and graph-based scene representations, isolating the role of input structure in spatial reasoning; and (4) we provide a large-scale procedurally generated benchmark with precise spatial annotations and counterfactual viewpoint queries to enable reproducible evaluation of spatial reasoning consistency.

## 2 Related Work

**Multimodal Large Language Models (MLLMs)**, such as GPT-4V/5 [29], Gemini [36], Qwen-VL [43], Kosmos-2 [30], and LLaVA [23], to name a few, have demonstrated strong performance in perception tasks such as captioning [1, 33], QA [3, 44], and grounding [41, 47]. Beyond generic VQA, a growing body of work explicitly targets fine-grained spatial grounding and structured reasoning. Groma [27] improves localized grounding through region-aware visual tokenization on benchmarks such as RefCOCO [50], while Ferret-v2 [51] and SpatialVLM [6] strengthen region-level and metric spatial reasoning via improved visual encoding and large-scale synthetic spatial supervision. Extensions into structured and 3D reasoning include LLaVA-ST [23], which addresses joint spatial-temporal grounding in video, and Struct2D [54], which leverages perception-guided structured inputs for 3D scene reasoning. SpatiaLQA [46] further highlights the difficulty of multi-step spatial logical reasoning in real-world indoor scenes. Collectively, these works demonstrate that modern MLLMs can localize, describe, and reason about spatial relations under direct observation and supervised settings. In contrast, our work probes whether such reasoning remains stable under counterfactual viewpoint transformation and extended sequential interaction, without additional perceptual input or task-specific adaptation.

**Benchmarks for multimodal perception** have provided a complementary view to task-driven benchmarks, by probing specific failure modes of multimodal models. Winoground-style compositional tests [37] and MMVP [40] reveal that strong VLMs can fail on fine-grained grounding distinctions. BLINK [13] exposes gaps in core perceptual reasoning beyond recognition, while HallusionBench [16] and POPE-style evaluations highlight hallucination, illusion, and logical inconsistency in image-conditioned generation. SEED-Bench-2-Plus [22] evaluates understanding of text-rich visual content, VLBiasBench [45] studies social bias in multimodal reasoning, and Vinoground [52] demonstrates brittleness in temporal and counterfactual reasoning over video. These benchmarks show that high aggregate VQA accuracy can mask systematic perceptual, compositional, or logical weaknesses. CVT-Bench extends this diagnostic perspective to spatial reasoning stability, isolating viewpoint-conditioned relational consistency under counterfactual transformation and accumulated interaction.

**Spatial understanding** has also been studied through compositional and embodied benchmarks. GQA [18], CLEVR [19], and NLVR2 [35] evaluate structured and compositional visual reasoning, while CLEVRER [49] highlights limitations in temporal and causal reasoning over dynamic scenes. Referring and

3D grounding datasets such as RefCOCO [50] and ScanRefer [7] extend spatial understanding to fine-grained localization in 2D and 3D environments. Embodied benchmarks including ALFRED [34], Habitat [32], and EmbodiedQA [11] require agents to integrate perception, spatial reasoning, and long-horizon planning in interactive environments. While these works demonstrate the importance of spatial state tracking in embodied settings, they couple spatial reasoning with navigation, action execution, or physical dynamics. CVT-Bench instead isolates viewpoint-conditioned relational persistence independently of planning or control, providing a controlled diagnostic of spatial state stability.

**Long-context and sequential reasoning** in large language and multi-modal models has been examined by a substantial body of research. LongBench [5], L-Eval [2], and RULER [17] show that effective performance often falls short of claimed context limits as input length and task complexity grow. Lost in the Middle [25] reveals strong positional biases in long sequences, while MuirBench [42] highlights weaknesses in multi-image reasoning. Interactive evaluations such as AgentBench [26] and AQA-Bench [48] further expose instability in stateful, multi-step reasoning. Memory augmentation approaches such as MemoryBank [53] attempt to mitigate long-horizon degradation through explicit memory mechanisms. These works establish that maintaining a consistent state over an extended context remains challenging. CVT-Bench contributes a targeted diagnostic within this landscape by isolating the persistence of viewpoint-conditioned spatial representations across multi-scene prompts, disentangling relational drift from downstream task performance.

### 3 CVT-Bench: Counterfactual Viewpoint Benchmark

**Task Definition.** We define counterfactual viewpoint spatial reasoning as the ability to infer spatial relationships between objects under hypothetical changes in observer viewpoint without additional visual observations. Let a scene be represented as a finite set of objects,  $\mathcal{S} = o_1, o_2, \dots, o_N$ , where each object  $o_i$  has a semantic label  $c_i$  and spatial position  $p_i \in \mathbb{R}^3$ . A viewpoint is defined by a camera pose  $v = (R, t)$ , where  $R \in SO(3)$  denotes rotation and  $t \in \mathbb{R}^3$  denotes translation. Under viewpoint  $v$ , the spatial relation between objects  $o_i$  and  $o_j$  is defined relative to the observer coordinate frame as  $r_{ij}^{(v)} \in \mathcal{R}$ , where  $\mathcal{R} = \text{left, right, front, behind}$  denotes the set of discrete spatial relations. Given an observed viewpoint  $v_0$ , we define a counterfactual viewpoint  $v_\theta$  obtained by rotating the observer by angle  $\theta$  about the vertical axis,  $v_\theta = (R_\theta R_0, t_0)$ , where  $R_\theta$  is the corresponding rotation operator. The model is not provided with visual observations from  $v_\theta$  and must instead infer spatial relations under this hypothetical transformation. Formally, the model receives input  $x = (\mathcal{O}, q)$ , where  $\mathcal{O}$  denotes a representation of the scene from viewpoint  $v_0$ , and  $q = (i, j, \theta)$  queries the spatial relation between objects  $o_i$  and  $o_j$  under rotation  $\theta$ . The model outputs a prediction  $\hat{r}_{ij}^{(v_\theta)} \subseteq \mathcal{R}$ .

**Evaluation Metrics.** We evaluate models in both episodic and sequential settings. In the episodic setting, each scene is presented independently, and

spatial reasoning is performed without prior context. In the sequential setting, multiple scenes appear within a shared interaction context through a single prompt, requiring models to maintain spatial state and avoid interference from prior observations. This distinction enables analysis of spatial reasoning stability both within individual scenes and across extended interaction. Spatial relationships in CVT-Bench are defined over a discrete set of directional predicates  $\mathcal{R} = \{\text{left, right, front, behind}\}$ . Due to the continuous spatial configuration of objects, multiple relationships may simultaneously hold between a pair of objects. For example, an object may be both to the front and to the right of another object under a given viewpoint. As a result, spatial relationship prediction is naturally formulated as a multi-label classification problem. Let  $r_{ij}^{(v_\theta)} \subseteq \mathcal{R}$  denote the ground truth set of spatial relationships between objects  $o_i$  and  $o_j$  under viewpoint  $v_\theta$ , and let  $\hat{r}_{ij}^{(v_\theta)} \subseteq \mathcal{R}$  denote the corresponding model prediction. We evaluate performance using precision and recall. Precision measures the correctness of predicted relationships, while recall measures the completeness of the predicted spatial relationships relative to the ground truth. These metrics ensure that models are evaluated both on their ability to identify valid spatial relationships and to recover the full relational structure between objects. In addition to per-query correctness, we introduce the notion of *spatial survival rate* to measure the stability of spatial reasoning across sequential interaction. Let a sequence of queries  $\{q_1, q_2, \dots, q_T\}$  be presented to the model within a shared interaction context. The survival rate at position  $t$  is defined as the probability that the model produces correct predictions until  $t$ , and is given by

$$\text{Survival}(t) = \frac{1}{N} \sum_{n=1}^N \prod_{k=1}^t \mathbb{I}(\hat{r}_{n,k} = r_{n,k}), \quad (1)$$

where  $N$  denotes the number of evaluated sequences and  $\mathbb{I}(\cdot)$  is the indicator function. This metric captures the degradation of spatial reasoning accuracy as interaction progresses, and provides a direct measure of the model’s ability to maintain stable spatial representations over extended context.

**Scene Generation and Benchmark Construction.** We construct *CVT-Bench* using procedurally generated scenes derived from the CLEVR environment [19], which provides controlled object geometry, semantic annotations, and precise spatial coordinates. CLEVR objects are chosen to ensure that all object categories, shapes, colors, sizes, and materials are familiar to multimodal models, allowing evaluation to focus on spatial reasoning rather than object recognition. Each object is assigned a unique identifier rendered on its surface, along with a dictionary mapping identifiers to semantic descriptions. This enables unambiguous object references in queries without requiring verbose bounding-box descriptions. We verified that all evaluated models achieve perfect accuracy in identifying tagged objects from the initial viewpoint, confirming that the benchmark does not introduce object recognition ambiguity.

We generate *100 scenes* using the original CLEVR rendering pipeline with objects placed on a tabletop plane. To study reasoning under varying com-

plexity, we construct two regimes: *sparse scenes* containing 3–5 objects and *dense scenes* containing 7–10 objects. Objects are randomly sampled from the CLEVR taxonomy and placed without stacking. Highly occluded objects are excluded from tags and queries, while partial occlusions are introduced through object placement, producing occlusion ratios between 5% and 70%. This enables evaluation under realistic visibility constraints while preserving object identifiability. Each scene is queried from viewpoints corresponding to rotations  $\theta \in \{0^\circ, 45^\circ, 90^\circ, 135^\circ, 180^\circ, 225^\circ, 270^\circ, 315^\circ, 360^\circ\}$  about the vertical axis, along with a bird’s-eye allocentric view. Spatial relationships between object pairs are computed from ground-truth 3D coordinates projected into the observer coordinate frame and discretized into predicates from  $\mathcal{R}$  following the CLEVR protocol. The original viewpoint includes 15 queries, while each additional viewpoint contains 5 queries generated by sampling object pairs and evaluating their relations under the corresponding viewpoint transformation. This yields up to 60 queries per scene (57 on average due to sparse scenes) and approximately 6,000 queries in total. To verify correctness, we manually inspected a randomly sampled subset of scenes. Two independent annotators confirmed spatial relation correctness.

**Query Generation and Counterfactual Viewpoint Protocol.** CVT-Bench evaluates spatial reasoning under *counterfactual viewpoint transformations* by querying models about object relations under hypothetical observer rotations. For each scene  $\mathcal{S}$ , spatial relations are defined relative to an initial viewpoint  $v_0$ . Counterfactual viewpoints are generated by rotating the observer about the vertical axis by  $\theta \in \{45^\circ, 90^\circ, 135^\circ, 180^\circ, 225^\circ, 270^\circ, 315^\circ, 360^\circ\}$ , as well as a bird’s-eye view, while preserving the underlying scene geometry. Models are not provided visual observations from these viewpoints and must instead infer the transformed spatial relations from their internal scene representation. For each viewpoint  $v_\theta$ , queries are generated by sampling ordered object pairs  $(o_i, o_j)$ . To measure spatial memory across interaction, we select *three relationships per scene* for sequential tracking, prioritizing occluded-object pairs for up to two of them. These relations appear across all *ten* viewpoints, allowing measurement of how long models maintain consistent spatial representations. Additionally, for the  $360^\circ$  viewpoint we reuse five queries from the original view with rephrased wording to measure *self-consistency*, since both viewpoints are identical.

Ground-truth relations  $r_{ij}^{(v_\theta)}$  are computed by transforming 3D object coordinates into the observer coordinate frame defined by  $v_\theta$  and discretizing relative positions<sup>1</sup> into predicates from  $\mathcal{R}$ . Each query asks for the spatial relation between two tagged objects under a specified viewpoint transformation, explicitly referencing object identifiers to eliminate ambiguity and ensure reasoning over spatial relations rather than object identity. Queries are generated for both the observed viewpoint  $v_0$  and counterfactual viewpoints  $v_\theta$ . Queries at  $v_0$  measure baseline spatial reasoning under direct observation, while counterfactual queries isolate the ability to transform spatial relations under hypothetical viewpoint changes. The range of rotation angles enables evaluation from small perspective

<sup>1</sup> Standard CLEVR protocol in Blender with angular threshold  $\varepsilon = 0.2$ .

shifts to complete viewpoint inversion. Beyond episodic evaluation, CVT-Bench includes a *sequential interaction protocol* in which scenes and queries appear within a continuous interaction context as a single prompt. Models must maintain spatial consistency across successive scenes and viewpoint transformations without resetting internal state. This protocol enables analysis of spatial reasoning stability under an extended context and reveals whether performance degradation is caused by contextual interference or the loss of spatial coherence.

## 4 Experimental Setup

**Models.** We evaluate a diverse set of state-of-the-art multimodal models spanning both closed- and open-source systems. Closed-source models include GPT-5.2 [29], Gemini-3.1 Pro [15,36], and Qwen-3.5 Plus [31], while open-source models include Qwen-3.5-397B-A17B [31] and Kimi-2.5 [20]. These models cover a range of parameter scales, context lengths, architectures and multimodal integration strategies, enabling analysis of spatial reasoning behavior across different model families. All models are evaluated in inference-only settings using publicly available interfaces without task-specific fine-tuning. We exclude Qwen-3-VL [4] and MolMo-2 [8] from our analysis after preliminary experiments exhibited degenerate response patterns under both episodic and sequential evaluation, producing invariant or near-invariant answers across queries regardless of scene configuration or viewpoint transformation. For GPT-5.2, we use a batch size of 10 (instead of 20 used for other models), as longer sequential interactions frequently exceeded the API output limit due to extensive reasoning tokens. Exact prompts, API configurations, and model details are in the appendix.

**Input Representations.** To study the role of representation structure in spatial reasoning, we evaluate each model under three input modalities: *visual*, *textual*, and *scene graph*. In the visual setting, models receive the rendered CLEVR scene with object identifier tags and a dictionary mapping tags to semantic descriptions. In the textual setting, the scene is provided as a structured natural language description listing objects and their spatial coordinates relative to the initial viewpoint, removing perceptual ambiguity and testing reasoning over symbolic descriptions. In the scene graph setting, the textual description is augmented with an explicit relational graph where objects are nodes and spatial relations are labeled edges derived from ground-truth coordinates. These representations allow us to distinguish failures arising from perception, representation structure, or internal reasoning. Additional prompt formatting details are provided in the appendix.

**Evaluation Protocol.** Performance is measured using F1 score to account for multi-label spatial relations. Furthermore, we report spatial survival rate (peak and from start) for tracking and consistency match rate for  $0^\circ=360^\circ$  agreement. We evaluate models under *episodic* and *sequential* interaction settings. In the episodic protocol, each scene and its queries are evaluated independently without prior context, measuring instantaneous spatial reasoning under both observed and counterfactual viewpoints. In the sequential protocol, scenes

and queries are concatenated into a single interaction context, requiring models to maintain spatial state across multiple independent scenes without resetting internal state. This setup avoids intermediate conversational turns, preventing models from using self-generated text as external memory and isolating passive context retention. Sequential reasoning is evaluated under batch sizes of 1 and 20 to analyze performance degradation as interaction length increases. Batch size 20 (10 for GPT) ensures substantial context accumulation while remaining well below model context limits, utilizing  $\sim 33\%$  of the available window for smaller models (Qwen+, Qwen-OS, Kimi) and  $\sim 10\%$  for larger models (Gemini and GPT-5.2). Thus performance reflects spatial state maintenance capability rather than context overflow.

**Counterfactual Viewpoint Evaluation.** For each scene, models answer queries at the observed viewpoint ( $\theta = 0^\circ$ ) and at rotated viewpoints. Observed-view queries measure baseline spatial reasoning under direct observation, while rotated queries evaluate the ability to transform spatial relations under hypothetical observer motion without additional visual input. This isolates viewpoint-conditioned reasoning and enables analysis of spatial consistency under increasing viewpoint transformation. We evaluate spatial reasoning across scene density and occlusion regimes to measure robustness under varying scene complexity. All experiments use recommended inference settings with *thinking* for each model. More details are in the appendix.

## 5 Results

**Episodic Spatial Reasoning Performance.** Figure 3 plots Global F1 as a function of viewpoint rotation under episodic evaluation, where each scene is presented independently without prior context. This setting isolates instantaneous spatial reasoning and the ability to infer spatial relations under counterfactual viewpoint transformations. Across models and representations, performance at the observed anchor viewpoint ( $\theta = 0^\circ$ ) is consistently higher than other views, with Gemini and GPT even exceeding 90% F1. This confirms that multimodal models reliably recover spatial relations under direct observation and that object identification and basic relational classification are not primary bottlenecks. However, performance degrades under counterfactual rotations, with notable drops around intermediate angles (e.g.,  $90^\circ$  and  $270^\circ$ ). Although some models partially recover at symmetric viewpoints ( $180^\circ$ ,  $360^\circ$ ), the overall trend indicates increasing difficulty as the observer frame diverges from the original view. Input representation influences this behavior. Text-only inputs often exhibit less degradation than image inputs, suggesting that part of the instability arises from multimodal grounding rather than purely geometric reasoning. Scene graph inputs alter performance in a model-dependent manner, occasionally stabilizing predictions. While single-view spatial reasoning is strong, maintaining consistent relational judgments under counterfactual observer motion remains fragile.

**Sequential Spatial Reasoning** We next evaluate spatial reasoning under sequential interaction, where multiple independent scenes are concatenated

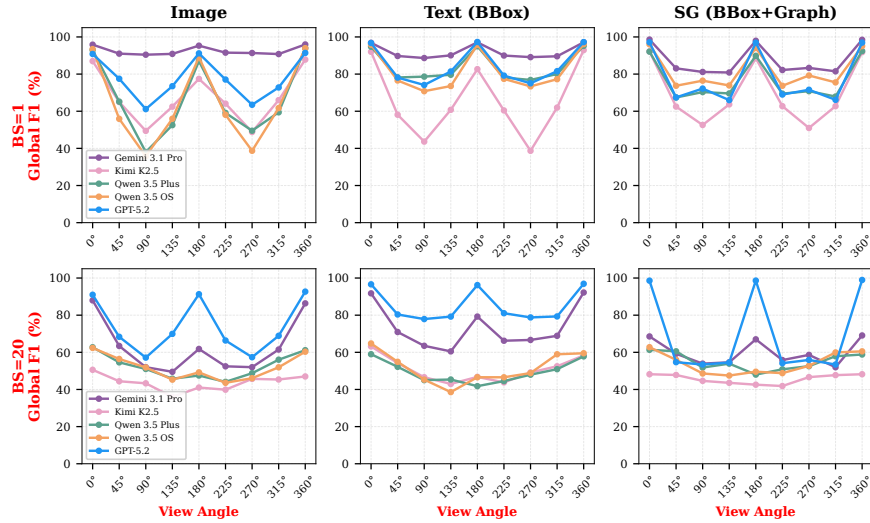


**Fig. 3:** Global F1 across viewpoint rotations for episodic (top) and sequential (bottom) evaluation under Image, Text-only, and Scene Graph inputs. The anchor viewpoint ( $0^\circ$ ) reflects direct spatial observation, while rotated viewpoints require counterfactual perspective transformation. Episodic performance is strong at  $0^\circ$ , but systematically degrades at intermediate rotations and declines further under sequential interaction. GPT-5.2 uses BS=10.

within a single prompt without intermediate resets. This protocol isolates the ability of models to maintain stable spatial representations across extended context, while avoiding semantic continuity across scenes. Because each scene is independent, any degradation reflects instability in spatial state maintenance rather than cross-scene narrative dependence. Moving from episodic evaluation to longer sequential interaction produces substantial performance degradation across models and representations, as seen in Figure 3. This drop affects both observed-view queries and counterfactual viewpoint transformations, indicating that sequential interaction undermines hypothetical perspective-taking and baseline relational inference, contrasting with episodic performance. This suggests that failure is due to a combination of poor geometric reasoning and reduced reliability under accumulated context.

**Contextual Stability** To probe persistence more directly, we analyze relational tracking across viewpoint sequences and visualize trends in Figure 4. We use the survival metric defined in Equation 1 to measure performance since aggregate F1 can mask any instability in maintaining a coherent relational state, as models intermittently answer correctly while failing to preserve consistent spatial structure over successive transformations. In the episodic setting, several models can sustain correct spatial relations over short stretches of the rotation cycle, though full-cycle stability remains limited. Under sequential evaluation, however, tracking survival collapses: long streak lengths become rare across model families

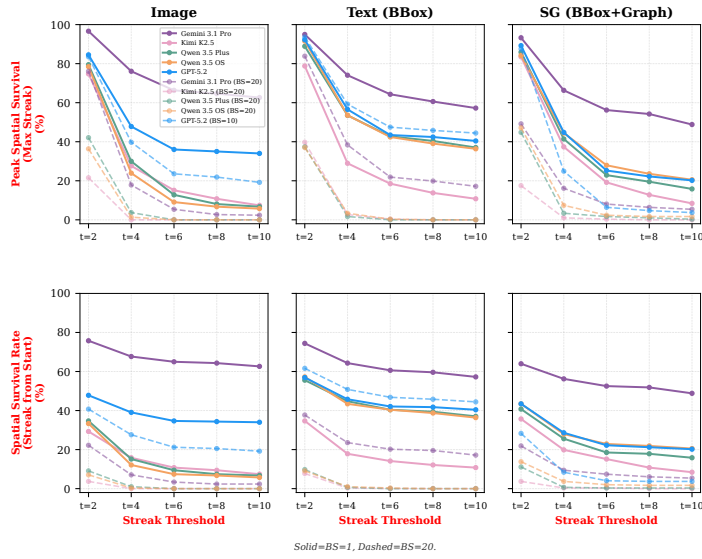


**Fig. 4:** Survival rate decay as a function of minimum consecutive-correct threshold  $t$  for peak survival (top) and survival from start (bottom), across Image, Text-only, and Scene Graph modalities. Solid lines indicate BS=1 (episodic); dashed lines indicate BS=20 (sequential). The monotonic decline quantifies how rapidly spatial reasoning coherence degrades as stricter consistency requirements are imposed. GPT-5.2 uses BS=10.

and input representations. This instability is further reflected in position-wise decay within the prompt (Figure 5). Performance systematically decreases with batch position: later scenes are answered less accurately than earlier ones, despite identical scene structure and query format. The decay pattern varies across representation, with Text-only inputs often exhibiting slower degradation than raw Image inputs, and Scene Graph representations exhibiting model-dependent behavior. These trends suggest that representation structure interacts with architectural memory mechanisms, influencing the robustness of spatial state retention under long context. Finally, we measure internal agreement under cycle consistency by re-asking a subset of  $0^\circ$  queries at  $360^\circ$  via paraphrase, where the underlying physical state is identical. In episodic evaluation, models typically exhibit high  $0^\circ=360^\circ$  agreement. Under extended sequential prompting, however, agreement declines with prompt depth, indicating erosion of self-consistency. The gap between episodic and long-context performance indicates that episodic accuracy does not reflect a stable, viewpoint-conditioned spatial representation.

**Counterfactual viewpoint reasoning** reveals structured, angle-dependent failure patterns that remain hidden under single-view accuracy, underscoring that reliable perspective taking requires more than high episodic spatial competence. Figure 3 shows performance as a function of counterfactual viewpoint angle, where models must infer spatial relations under discrete rotations  $\theta \in$

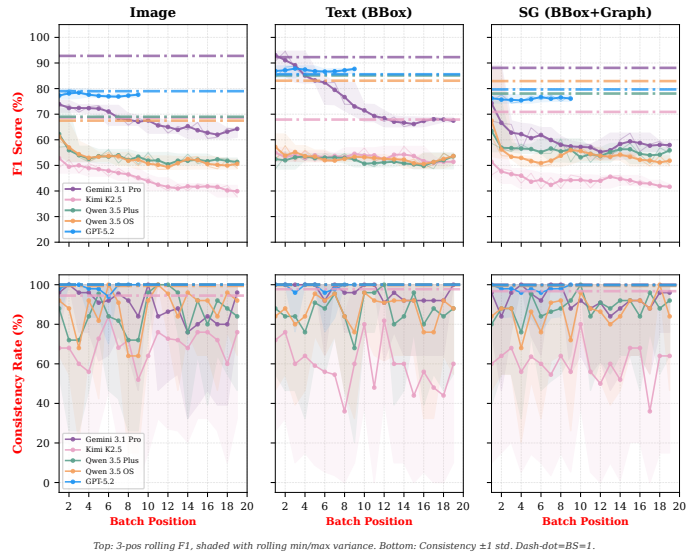


**Fig. 5: Performance and sequential stability across input representations.** Top: Global F1 decay across batch positions. Bottom:  $0^\circ=360^\circ$  consistency match rate drift across prompt depth, with shaded regions showing  $\pm 1$  standard deviation. While models achieve strong episodic performance, spatial consistency degrades under sequential interaction, indicating instability in maintaining spatial state. GPT-5.2 uses BS=10.

$45^\circ, 90^\circ, \dots, 360^\circ$  and a top-down allocentric view without additional visual input. Across models and representations, F1 generally decreases as the target viewpoint diverges from the observed  $0^\circ$  anchor, yielding a characteristic U- or V-shaped profile that reflects the increasing difficulty of perspective transformation relative to direct observation. However, this degradation is not uniformly smooth: several models (including Kimi 2.5, Qwen 3.5 Plus, Qwen 3.5 OS, and GPT-5.2) exhibit disproportionate drops at orthogonal angles ( $90^\circ$  and  $270^\circ$ ), frequently recovering significantly at  $180^\circ$ , suggesting brittle or heuristic transformation strategies rather than a stable internal rotation of relational state. Surprisingly, performance remains highly robust for top-down allocentric queries, consistently outperforming orthogonal in-plane rotations and often rivaling the  $0^\circ$  baseline; this indicates that models may find vertical, top-down spatial projections significantly easier to map than severe egocentric horizontal-plane rotations. Representation choice modulates these effects: Text-only inputs often reduce overall degradation relative to Image by providing explicit geometric structure, while Scene Graph representations produce model-dependent improvements or regressions, highlighting strong interactions between representation format and architectural mechanisms for spatial transformation.

**Effect of Scene Complexity and Occlusion.** Figure 6 stratifies performance by scene density (Sparse vs. Dense) and visibility (Fully Visible vs.

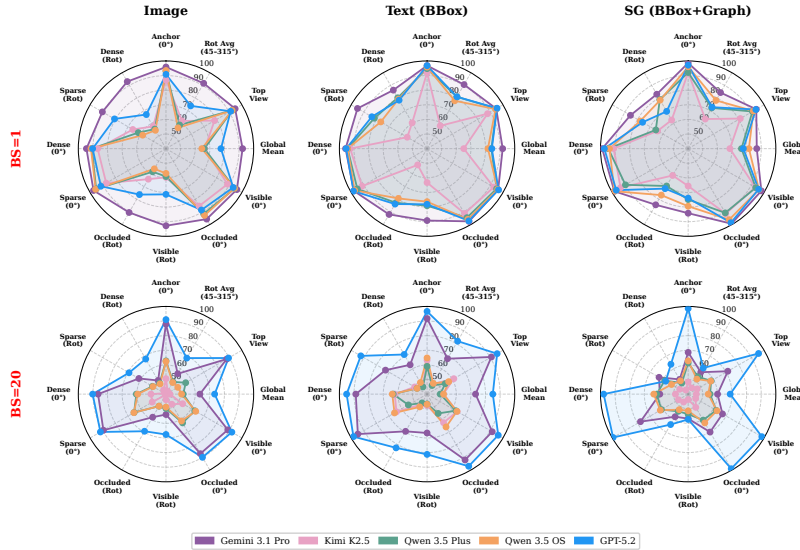


**Fig. 6:** Multi-dimensional performance summarizing model competence across twelve axes: anchor F1 ( $0^\circ$ ), rotation F1 (mean over  $45^\circ$ – $315^\circ$ ), top-down perspective, global F1, and visual complexity (dense vs. sparse, visible vs. occluded) broken down by ( $0^\circ$ ) vs rotation. Top: episodic evaluation (BS=1); bottom: sequential evaluation (BS=20, 10 for GPT).

Partially Occluded) cases. At the anchor viewpoint ( $0^\circ$ ), models exhibit the expected difficulty gradient: sparse and fully visible scenes outperform dense and occluded configurations across representations. Under counterfactual rotations, however, the structure of these gradients diverges. The performance gap between visible and occluded targets compresses substantially in Image mode—where occluded queries occasionally match or exceed visible performance under rotation—indicating that viewpoint stress overrides sensitivity to initial visibility. Conversely, the difficulty gap between sparse and dense scenes actually widens under rotation in Image mode, demonstrating that high distractor load heavily exacerbates the difficulty of perspective transformation. Interestingly, when relying on explicit geometric representations (Text-Only), models suffer from density paradoxes where sparse scenes occasionally underperform dense ones under rotational stress.

While increased scene complexity reduces spatial reasoning reliability, counterfactual viewpoint transformations often collapse these differences, indicating that models struggle to preserve viewpoint-conditioned relational structure.

**Failure Modes.** We analyze qualitative and quantitative error patterns to better understand the mechanisms underlying spatial degradation. A recurring pattern across models is viewpoint inversion, where left/right or front/behind relations are systematically confused under rotation, particularly at orthogonal angles ( $90^\circ$  and  $270^\circ$ ). These errors are not uniformly distributed across view-

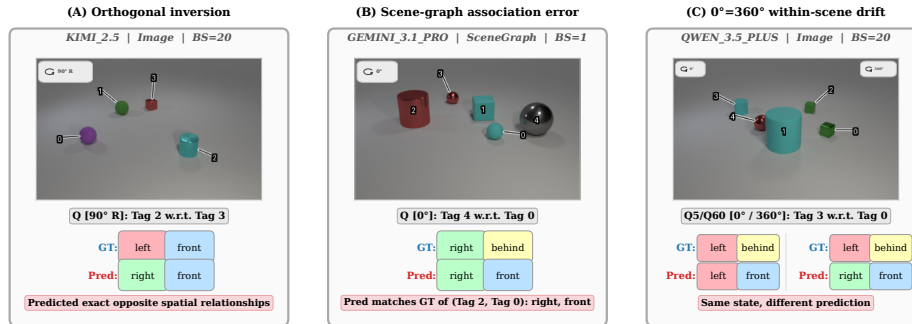


**Fig. 7: Qualitative failure modes in CVT-Bench.** (A) **Orthogonal inversion:**  $90^\circ$  rotations can flip left/right relations (GT={left, front}, Pred={right, front}). (B) **Scene-graph mis-association:** predictions match the relation of a different object pair in the scene. (C) **Within-scene drift:** predictions differ between  $0^\circ$  and  $360^\circ$  queries despite identical physical states.

points but cluster at specific rotations, producing sharp, angle-localized drops that are consistent with brittle or heuristic transformation strategies rather than smooth internal rotation of spatial state. Under structured inputs, additional failure modes emerge: Scene Graph representations can induce relation-association errors in which models misattribute predicates to incorrect object pairs or partially invert relational structure in non-systematic ways. These errors are often less coherent than simple left-right swaps and suggest difficulty in reliably parsing and grounding explicitly encoded relational structure. In the sequential setting, error patterns increasingly reflect cross-scene interference, where responses become less sensitive to the geometry of the current scene and more variable with prompt depth, consistent with contextual drift in a shared interaction window.

## 6 Conclusion and Future Work

We introduced *CVT-Bench*, a diagnostic benchmark for evaluating spatial reasoning in multimodal models under counterfactual viewpoint transformations and extended sequential interaction. While modern MLLMs achieve high accuracy under direct observation, our results show consistent degradation under viewpoint rotation and long-context interaction, indicating that spatial reasoning is often view-dependent rather than based on stable relational representations. CVT-Bench further reveals model-specific stability profiles and heterogeneous sensitivity to input representation, demonstrating that spatial consistency emerges from interactions between architecture, representation structure, and interaction length. Through extensive experiments, we conclude that reliable spatial reasoning in multimodal models is not merely a perception problem, but a challenge of maintaining stable spatial representations across viewpoints and time. Future work will extend this evaluation to more complex real-world environments and embodied settings where spatial state must be maintained through

action and perception. Ultimately, improving spatial reasoning in multimodal systems may require explicit mechanisms for relational state representation.

**Acknowledgement.** This research was supported in part by the US National Science Foundation grants IIS 2348689 and IIS 2348690.

## References

1. Agrawal, H., Desai, K., Wang, Y., Chen, X., Jain, R., Johnson, M., Batra, D., Parikh, D., Lee, S., Anderson, P.: Nocaps: Novel object captioning at scale. In: Proceedings of the IEEE/CVF international conference on computer vision. pp. 8948–8957 (2019)
2. An, C., Gong, S., Zhong, M., Zhao, X., Li, M., Zhang, J., Kong, L., Qiu, X.: L-eval: Instituting standardized evaluation for long context language models (2023), <https://arxiv.org/abs/2307.11088>
3. Antol, S., Agrawal, A., Lu, J., Mitchell, M., Batra, D., Zitnick, C.L., Parikh, D.: Vqa: Visual question answering. In: Proceedings of the IEEE International Conference on Computer Vision. pp. 2425–2433 (2015)
4. Bai, S., Cai, Y., Chen, R., Chen, K., Chen, X., Cheng, Z., Deng, L., Ding, W., Gao, C., Ge, C., Ge, W., Guo, Z., Huang, Q., Huang, J., Huang, F., Hui, B., Jiang, S., Li, Z., Li, M., Li, M., Li, K., Lin, Z., Lin, J., Liu, X., Liu, J., Liu, C., Liu, Y., Liu, D., Liu, S., Lu, D., Luo, R., Lv, C., Men, R., Meng, L., Ren, X., Ren, X., Song, S., Sun, Y., Tang, J., Tu, J., Wan, J., Wang, P., Wang, P., Wang, Q., Wang, Y., Xie, T., Xu, Y., Xu, H., Xu, J., Yang, Z., Yang, M., Yang, J., Yang, A., Yu, B., Zhang, F., Zhang, H., Zhang, X., Zheng, B., Zhong, H., Zhou, J., Zhou, F., Zhou, J., Zhu, Y., Zhu, K.: Qwen3-vl technical report (2025), <https://arxiv.org/abs/2511.21631>
5. Bai, Y., Lv, X., Zhang, J., Lyu, H., Tang, J., Huang, Z., Du, Z., Liu, X., Zeng, A., Hou, L., Dong, Y., Tang, J., Li, J.: Longbench: A bilingual, multitask benchmark for long context understanding (2024), <https://arxiv.org/abs/2308.14508>
6. Chen, B., Xu, Z., Kirmani, S., Ichter, B., Sadigh, D., Guibas, L., Xia, F.: Spatialvlm: Endowing vision-language models with spatial reasoning capabilities. In: Proceedings of the IEEE/CVF Conference on Computer Vision and Pattern Recognition. pp. 14455–14465 (2024)
7. Chen, D.Z., Chang, A.X., Nießner, M.: Scanrefer: 3d object localization in rgb-d scans using natural language (2020), <https://arxiv.org/abs/1912.08830>
8. Clark, C., Zhang, J., Ma, Z., Park, J.S., Salehi, M., Tripathi, R., Lee, S., Ren, Z., Kim, C.D., Yang, Y., Shao, V., Yang, Y., Huang, W., Gao, Z., Anderson, T., Zhang, J., Jain, J., Stoica, G., Han, W., Farhadi, A., Krishna, R.: Molmo2: Open weights and data for vision-language models with video understanding and grounding (2026), <https://arxiv.org/abs/2601.10611>
9. Cui, C., Ma, Y., Cao, X., Ye, W., Zhou, Y., Liang, K., Chen, J., Lu, J., Yang, Z., Liao, K.D., et al.: A survey on multimodal large language models for autonomous driving. In: Proceedings of the IEEE/CVF Winter Conference on Applications of Computer Vision. pp. 958–979 (2024)
10. Cui, C., Yang, Z., Zhou, Y., Ma, Y., Lu, J., Li, L., Chen, Y., Panchal, J., Wang, Z.: Personalized autonomous driving with large language models: Field experiments. In: 2024 IEEE 27th International Conference on Intelligent Transportation Systems (ITSC). pp. 20–27. IEEE (2024)
11. Das, A., Datta, S., Gkioxari, G., Lee, S., Parikh, D., Batra, D.: Embodied question answering (2017), <https://arxiv.org/abs/1711.11543>

12. Deitke, M., Clark, C., Lee, S., Tripathi, R., Yang, Y., Park, J.S., Salehi, M., Muenighoff, N., Lo, K., Soldaini, L., et al.: Molmo and pixmo: Open weights and open data for state-of-the-art vision-language models. In: Proceedings of the Computer Vision and Pattern Recognition Conference. pp. 91–104 (2025)
13. Fu, X., Hu, Y., Li, B., Feng, Y., Wang, H., Lin, X., Roth, D., Smith, N.A., Ma, W.C., Krishna, R.: Blink: Multimodal large language models can see but not perceive. In: European Conference on Computer Vision. pp. 148–166. Springer (2024)
14. Fung, A., Tan, A.H., Wang, H., Benhabib, B., Nejat, G.: Mllm-search: A zero-shot approach to finding people using multimodal large language models. *Robotics* **14**(8), 102 (2025)
15. Google DeepMind: Gemini 3.1 Pro model card. Tech. rep., Google (February 2026), <https://deepmind.google/models/model-cards/gemini-3-1-pro/>, public Preview released Feb 19, 2026
16. Guan, T., Liu, F., Wu, X., Xian, R., Li, Z., Liu, X., Wang, X., Chen, L., Huang, F., Yacoob, Y., et al.: Hallusionbench: an advanced diagnostic suite for entangled language hallucination and visual illusion in large vision-language models. In: Proceedings of the IEEE/CVF Conference on Computer Vision and pattern recognition. pp. 14375–14385 (2024)
17. Hsieh, C.P., Sun, S., Krizan, S., Acharya, S., Rekesh, D., Jia, F., Zhang, Y., Ginsburg, B.: Ruler: What’s the real context size of your long-context language models? (2024), <https://arxiv.org/abs/2404.06654>
18. Hudson, D.A., Manning, C.D.: Gqa: A new dataset for real-world visual reasoning and compositional question answering (2019), <https://arxiv.org/abs/1902.09506>
19. Johnson, J., Hariharan, B., van der Maaten, L., Fei-Fei, L., Zitnick, C.L., Girshick, R.: Clevr: A diagnostic dataset for compositional language and elementary visual reasoning (2016), <https://arxiv.org/abs/1612.06890>
20. Kimi 2.5 Team: Kimi K2.5 (February 2026), <https://huggingface.co/moonshotai/Kimi-K2.5>, version 2.5, released Feb 2, 2026
21. Krishna, R., Zhu, Y., Groth, O., Johnson, J., Hata, K., Kravitz, J., Chen, S., Kalantidis, Y., Li, L.J., Shamma, D.A., et al.: Visual genome: Connecting language and vision using crowdsourced dense image annotations. *International Journal of Computer Vision* **123**(1), 32–73 (2017)
22. Li, B., Ge, Y., Chen, Y., Ge, Y., Zhang, R., Shan, Y.: Seed-bench-2-plus: Benchmarking multimodal large language models with text-rich visual comprehension. arXiv preprint arXiv:2404.16790 (2024)
23. Li, H., Chen, J., Wei, Z., Huang, S., Hui, T., Gao, J., Wei, X., Liu, S.: Llava-st: A multimodal large language model for fine-grained spatial-temporal understanding. In: Proceedings of the IEEE/CVF Conference on Computer Vision and Pattern Recognition. pp. 8592–8603 (2025)
24. Li, X., Zhang, M., Geng, Y., Geng, H., Long, Y., Shen, Y., Zhang, R., Liu, J., Dong, H.: Manipllm: Embodied multimodal large language model for object-centric robotic manipulation. In: Proceedings of the IEEE/CVF Conference on Computer Vision and Pattern Recognition. pp. 18061–18070 (2024)
25. Liu, N.F., Lin, K., Hewitt, J., Paranjape, A., Bevilacqua, M., Petroni, F., Liang, P.: Lost in the middle: How language models use long contexts (2023), <https://arxiv.org/abs/2307.03172>
26. Liu, X., Yu, H., Zhang, H., Xu, Y., Lei, X., Lai, H., Gu, Y., Ding, H., Men, K., Yang, K., Zhang, S., Deng, X., Zeng, A., Du, Z., Zhang, C., Shen, S., Zhang, T., Su, Y., Sun, H., Huang, M., Dong, Y., Tang, J.: Agentbench: Evaluating llms as agents (2025), <https://arxiv.org/abs/2308.03688>

27. Ma, C., Jiang, Y., Wu, J., Yuan, Z., Qi, X.: Groma: Localized visual tokenization for grounding multimodal large language models. In: European Conference on Computer Vision. pp. 417–435. Springer (2024)
28. Michelon, P., Zacks, J.M.: Two kinds of visual perspective taking. *Perception & psychophysics* **68**(2), 327–337 (2006)
29. OpenAI: Update to GPT-5 system card: GPT-5.2. Tech. rep., OpenAI (December 2025), [https://cdn.openai.com/pdf/3a4153c8-c748-4b71-8e31-aecbde944f8d/oai\\_5\\_2\\_system-card.pdf](https://cdn.openai.com/pdf/3a4153c8-c748-4b71-8e31-aecbde944f8d/oai_5_2_system-card.pdf), accessed: 2026-03-03
30. Peng, Z., Wang, W., Dong, L., Hao, Y., Huang, S., Ma, S., Wei, F.: Kosmos-2: Grounding multimodal large language models to the world. arXiv preprint arXiv:2306.14824 (2023)
31. Qwen Team: Qwen 3.5 Plus: Towards native multimodal agents (February 2026), <https://qwen.ai/blog?id=qwen3.5>, version 3.5 Plus, released Feb 13, 2026
32. Savva, M., Kadian, A., Maksymets, O., Zhao, Y., Wijmans, E., Jain, B., Straub, J., Liu, J., Koltun, V., Malik, J., Parikh, D., Batra, D.: Habitat: A platform for embodied ai research (2019), <https://arxiv.org/abs/1904.01201>
33. Sharma, P., Ding, N., Goodman, S., Soricut, R.: Conceptual captions: A cleaned, hypertexted, image alt-text dataset for automatic image captioning. In: Proceedings of the 56th Annual Meeting of the Association for Computational Linguistics (Volume 1: Long Papers). pp. 2556–2565 (2018)
34. Shridhar, M., Thomason, J., Gordon, D., Bisk, Y., Han, W., Mottaghi, R., Zettlemoyer, L., Fox, D.: Alfred: A benchmark for interpreting grounded instructions for everyday tasks (2020), <https://arxiv.org/abs/1912.01734>
35. Suhr, A., Zhou, S., Zhang, A., Zhang, I., Bai, H., Artzi, Y.: A corpus for reasoning about natural language grounded in photographs (2019), <https://arxiv.org/abs/1811.00491>
36. Team, G., Anil, R., Borgeaud, S., Alayrac, J.B., Yu, J., Soricut, R., Schalkwyk, J., Dai, A.M., Hauth, A., Millican, K., et al.: Gemini: a family of highly capable multimodal models. arXiv preprint arXiv:2312.11805 (2023)
37. Thrush, T., Jiang, R., Bartolo, M., Singh, A., Williams, A., Kiela, D., Ross, C.: Winoground: Probing vision and language models for visio-linguistic compositionality. In: Proceedings of the IEEE/CVF Conference on Computer Vision and Pattern Recognition. pp. 5238–5248 (2022)
38. Tian, M., Luo, T., Ding, J., Wang, X., Cheung, H.: Spatial ability and theory of mind: A mediating role of visual perspective taking. *Child Development* **92**(4), 1590–1604 (2021)
39. Tian, X., Gu, J., Li, B., Liu, Y., Wang, Y., Zhao, Z., Zhan, K., Jia, P., Lang, X., Zhao, H.: Drivevlm: The convergence of autonomous driving and large vision-language models. arXiv preprint arXiv:2402.12289 (2024)
40. Tong, S., Liu, Z., Zhai, Y., Ma, Y., LeCun, Y., Xie, S.: Eyes wide shut? exploring the visual shortcomings of multimodal llms. In: Proceedings of the IEEE/CVF Conference on Computer Vision and pattern recognition. pp. 9568–9578 (2024)
41. Wang, C., Feng, W., Li, X., Cheng, G., Lyu, S., Liu, B., Chen, L., Zhao, Q.: Ov-vg: A benchmark for open-vocabulary visual grounding. *Neurocomputing* **591**, 127738 (2024)
42. Wang, F., Fu, X., Huang, J.Y., Li, Z., Liu, Q., Liu, X., Ma, M.D., Xu, N., Zhou, W., Zhang, K., Yan, T.L., Mo, W.J., Liu, H.H., Lu, P., Li, C., Xiao, C., Chang, K.W., Roth, D., Zhang, S., Poon, H., Chen, M.: Muirbench: A comprehensive benchmark for robust multi-image understanding (2024), <https://arxiv.org/abs/2406.09411>

43. Wang, P., Bai, S., Tan, S., Wang, S., Fan, Z., Bai, J., Chen, K., Liu, X., Wang, J., Ge, W., et al.: Qwen2-vl: Enhancing vision-language model’s perception of the world at any resolution. arXiv preprint arXiv:2409.12191 (2024)
44. Wang, P., Wu, Q., Shen, C., Dick, A., Van Den Hengel, A.: Fvqa: Fact-based visual question answering. *IEEE Transactions on Pattern Analysis and Machine Intelligence* **40**(10), 2413–2427 (2017)
45. Wang, S., Cao, X., Zhang, J., Yuan, Z., Shan, S., Chen, X., Gao, W.: Vlbiasbench: A comprehensive benchmark for evaluating bias in large vision-language model. arXiv preprint arXiv:2406.14194 (2024)
46. Xie, Y., Zhang, X., Shan, Y., Zhu, H., Tang, R., Wei, R., Song, M., Wan, Y., Song, J.: Spatialqa: A benchmark for evaluating spatial logical reasoning in vision-language models. arXiv preprint arXiv:2602.20901 (2026)
47. Xu, Y., Zhu, L., Yang, Y.: Mc-bench: A benchmark for multi-context visual grounding in the era of mllms. In: *Proceedings of the IEEE/CVF International Conference on Computer Vision*. pp. 17675–17687 (2025)
48. Yang, S., Zhao, B., Xie, C.: Aqa-bench: An interactive benchmark for evaluating llms’ sequential reasoning ability (2025), <https://arxiv.org/abs/2402.09404>
49. Yi, K., Gan, C., Li, Y., Kohli, P., Wu, J., Torralba, A., Tenenbaum, J.B.: Clevrer: Collision events for video representation and reasoning (2020), <https://arxiv.org/abs/1910.01442>
50. Yu, L., Poirson, P., Yang, S., Berg, A.C., Berg, T.L.: Modeling context in referring expressions (2016), <https://arxiv.org/abs/1608.00272>
51. Zhang, H., You, H., Dufter, P., Zhang, B., Chen, C., Chen, H.Y., Fu, T.J., Wang, W.Y., Chang, S.F., Gan, Z., et al.: Ferret-v2: An improved baseline for referring and grounding with large language models. arXiv preprint arXiv:2404.07973 (2024)
52. Zhang, J., Cai, M., Lee, Y.J.: Vinoground: Scrutinizing llms over dense temporal reasoning with short videos. arXiv preprint arXiv:2410.02763 (2024)
53. Zhong, W., Guo, L., Gao, Q., Ye, H., Wang, Y.: Memorybank: Enhancing large language models with long-term memory (2023), <https://arxiv.org/abs/2305.10250>
54. Zhu, F., Wang, H., Xie, Y., Gu, J., Ding, T., Yang, J., Jiang, H.: Struct2d: A perception-guided framework for spatial reasoning in mllms. arXiv preprint arXiv:2506.04220 (2025)

## 7 Appendix A

This appendix provides additional dataset statistics, expanded results figures and tables omitted from the main paper due to space constraints, and reproducibility details including prompt templates and API settings. The goal is twofold: first, to expose finer-grained quantitative trends underlying the main-paper results; and second, to document implementation details needed to reproduce CVT-Bench evaluation across all input representations and models.

### Contents.

- **Dataset details:** CVT-Bench composition and statistics (Table S1).
- **Extended results:** batch-size effects (Fig. S1), density/occlusion breakdowns (Fig. S2), universally hard questions (Fig. S3, Table S2), and additional analyses on relation-axis asymmetry, top-view versus orbit-view reasoning, and cross-model failure overlap.
- **Model/system profile:** context and token utilization (Table S3).
- **Reproducibility:** prompt templates and API settings (Sec. 11).

## 8 Dataset Details

### 8.1 CVT-Bench Composition and Statistics

Table S1 summarizes CVT-Bench composition across scenes, views, and query types. The benchmark contains 100 CLEVR-style tabletop scenes split evenly between sparse (3–5 objects) and dense (7–10 objects) configurations, yielding an average of 6.2 objects per scene after visibility filtering. Each scene is queried from ten viewpoints (nine azimuth rotations plus a top-down view), producing 5,703 total questions (57.0 per scene on average; up to 60). Most questions are counterfactual manipulations (77.5%), while 22.5% are standard queries at the original view ( $0^\circ$ ). Occlusion is present in 43% of scenes and affects 23.1% of questions; the table also breaks occlusion down by whether the subject, object, or both are occluded. Finally, because spatial relations are multi-label (typically one lateral and one depth predicate), 97.5% of questions contain multiple labels, with 11,263 total relation labels across the dataset. This table provides the dataset-level context for interpreting performance differences across density, occlusion, and viewpoint.

Property	Value	Details
<b>Scene composition</b>		
Sparse scenes	50	3–5 placed objects (min 2 after visibility filtering)
Dense scenes	50	7–10 placed objects
Objects per scene (all)	6.2 avg	min 2, max 10
<b>Questions</b>		
Total questions	5,703	mean 57.0/scene (min 20, max 60)
Standard (original view)	1,284 (22.5%)	$\theta = 0^\circ$ ; no counterfactual rotation
Manipulation (rotated/top)	4,419 (77.5%)	$\theta \in \{45^\circ, \dots, 360^\circ\}$ + top-down
<b>Occlusion</b>		
Scenes with occlusion	43/100 (43%)	mean 13.2 occluded questions/scene (max 43)
Occluded questions	1,315 (23.1%)	subj 613   obj 620   both 82
Visible questions	4,388 (76.9%)	no occlusion involvement
<b>Relationship labels</b>		
Directions	4	left/right/front/behind (nearly uniform)
Multi-label questions	5,560 (97.5%)	typically 2 relations/query (L/R + F/B)
Total relation labels	11,263	$\sim 2.0$ labels/query on average
<b>Views</b>		
View angles	10	$0^\circ, 45^\circ\text{--}315^\circ$ (8), $360^\circ$ , top-down
Image size	$320 \times 240$	CLEVR-rendered images

**Table S1:** CVT-Bench composition and design parameters: number of scenes, view-point angles, density levels (Sparse / Dense), occlusion conditions (Visible / Occluded), total questions, and relation label types. Most questions require a lateral (Left / Right) and a depth (Front / Behind) judgment, yielding a multi-label classification task with up to two labels per question.

## 9 Extended Results

### 9.1 Batch Size Effects: Episodic vs. Sequential Performance

Figure S1 isolates the context penalty incurred when transitioning from episodic evaluation (BS=1) to sequential evaluation (BS=20), where multiple independent scenes are concatenated in a single prompt. The paired bars show that Global F1 typically drops under sequential prompting across models and representations, indicating that long-context interaction introduces interference beyond single-scene spatial reasoning difficulty. The relative gap between BS=1

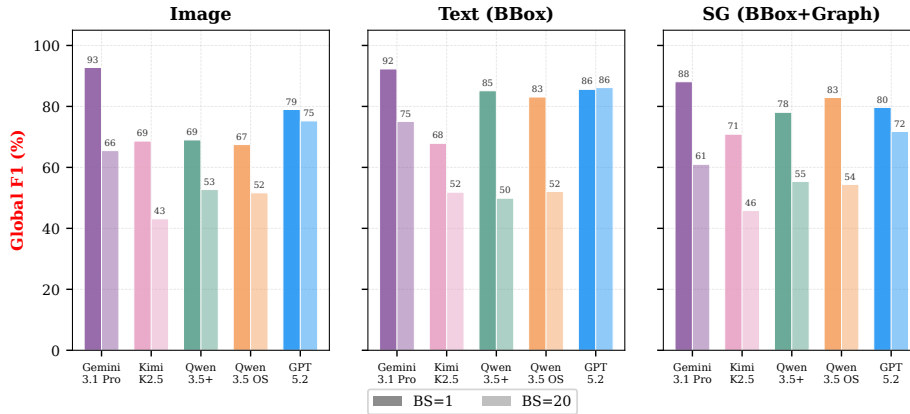


**Fig. S1:** Global F1 comparison between episodic (BS=1) and sequential (BS=20) evaluation across all models and input modalities. Each bar pair isolates the effect of context accumulation: the difference between dark (BS=1) and light (BS=20) bars quantifies the context-length penalty incurred when processing 20 scenes within a single prompt versus evaluating each scene independently. GPT-5.2 uses batch size 10.

and BS=20 provides a compact summary of each model’s sensitivity to context accumulation and cross-scene interference.

## 9.2 Difficulty Slices: Density and Occlusion

Figure S2 breaks performance down along two axes of visual complexity: scene density (Sparse vs. Dense) and visibility (Visible vs. Occluded), under both episodic and sequential settings. While many models perform better on sparse and visible configurations at the anchor view, the figure highlights regimes where the expected difficulty ordering compresses or inverts under sequential prompting and viewpoint stress. The triangle markers flag such paradoxes, which are consistent with heuristic fallback behavior: when rotation or long-context interference dominates, models may rely less on grounded geometric evidence, erasing the typical gap between easy and hard conditions.

## 9.3 Context Length and Spatial State Degradation

This section provides additional context for sequential degradation trends. Although sequential prompts can be long, the observed failures are not explained solely by exhausting context windows: across models, BS=20 prompts occupy only a fraction of the available context capacity, yet performance still drops sharply with increasing batch size. Moreover, degradation is structured within a prompt: later scenes are answered less reliably than earlier ones despite identical formatting, suggesting positional interference and cross-scene contamination rather than isolated hard cases. Together, these observations indicate that the limiting factor is the ability to maintain and multiplex spatial state across

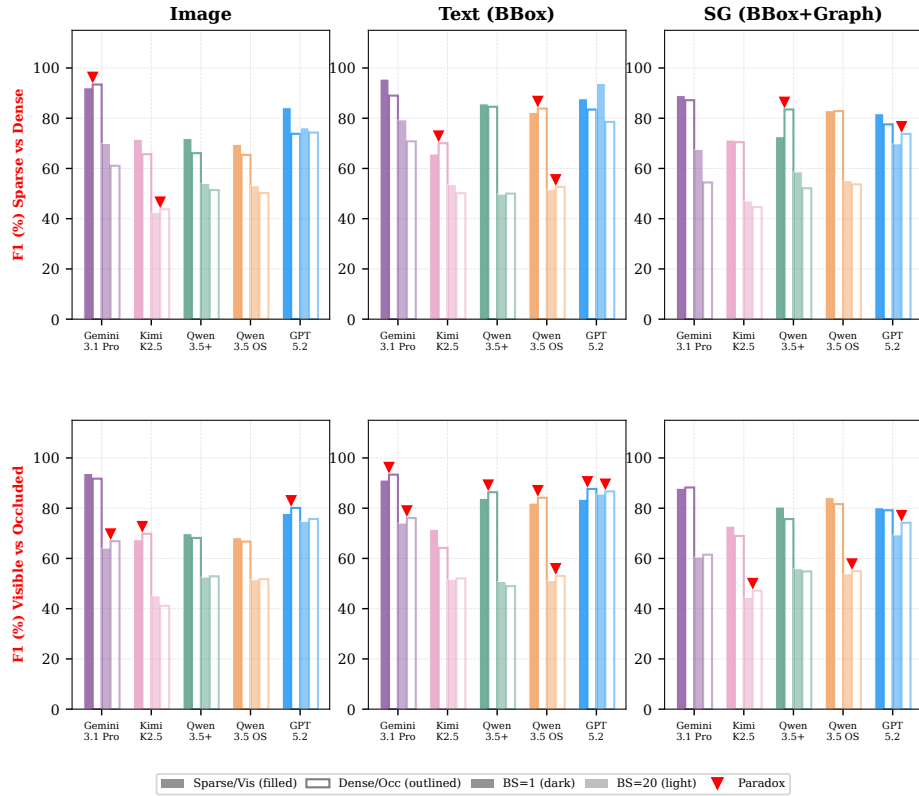


**Fig. S2:** Performance breakdown by scene difficulty dimensions: scene density (top row: Sparse vs Dense) and object visibility (bottom row: Visible vs Occluded), evaluated across both BS=1 and BS=20. Solid bars represent the easier condition (Sparse / Visible); hatched bars represent the harder condition (Dense / Occluded). Triangle markers flag paradoxes where a model performs better on the harder condition. GPT-5.2 uses batch size 10.

independent episodes within a shared context, not simply truncation or a hard context-length ceiling. Exact token utilization statistics are reported in Table S3.

#### 9.4 Universal Hard Cases

Figure S3 and Table S2 characterize universally hard questions, i.e., benchmark items that all evaluated models answer incorrectly under a given condition. The qualitative montage provides representative examples across viewpoints and scene regimes, illustrating failures that persist even under clean synthetic rendering and unambiguous tagging. Quantitatively, the prevalence of universally hard questions increases sharply under sequential prompting for all three representations, confirming that shared failure modes become more common as context accumulates. In Image mode, the proportion rises from 7.9% at BS=1 to 19.3% at BS=20, while SceneGraph shows a similarly large increase from 6.4% to 16.0%.

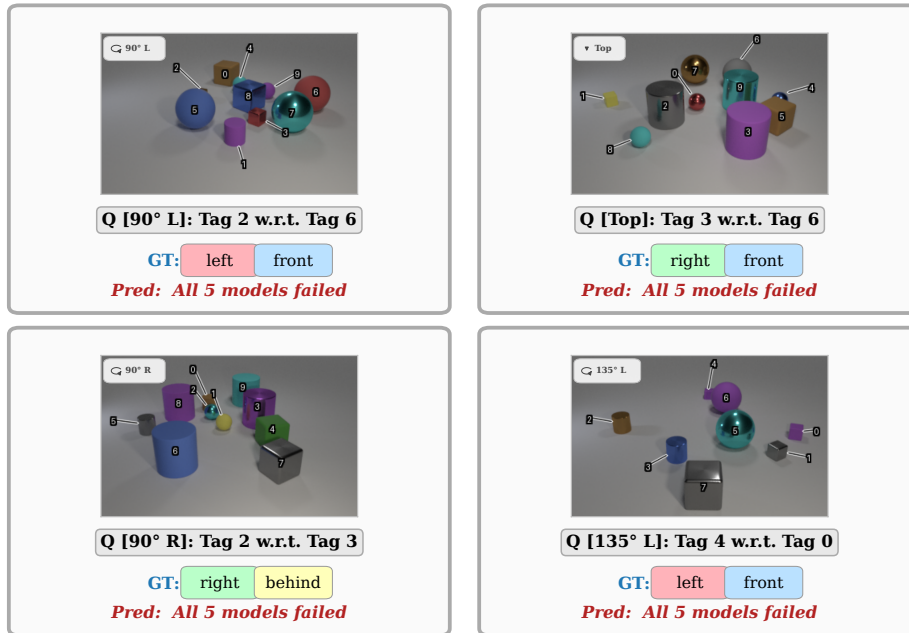


**Fig. S3: Universal hard cases.** A montage of queries that are failed by all evaluated models under the specified setting. Each cell shows the anchor image with tags, the queried counterfactual viewpoint, and the ground-truth relations.

Condition	Count	% of Total
BS=1  Image	449	7.9%
BS=20  Image	1102	19.3%
BS=1  Text-Only	605	10.6%
BS=20  Text-Only	766	13.4%
BS=1  SceneGraph	366	6.4%
BS=20  SceneGraph	912	16.0%

**Table S2:** Count and percentage of questions that all models answer incorrectly, stratified by evaluation condition.

Text-only remains comparatively more robust, but still exhibits a noticeable rise from 10.6% to 13.4%. Interestingly, SceneGraph has the lowest universally hard rate in the episodic setting, but loses much of this advantage under long-context evaluation. Overall, these results reinforce the main paper’s conclusion that context accumulation induces not only lower average accuracy, but also a growing subset of questions that systematically defeat all models.

## 9.5 Relation-Axis Asymmetry Under Context Load

A more fine-grained breakdown by relation type reveals that counterfactual viewpoint reasoning is not uniformly difficult across spatial predicates. Across models,

*left/right* judgments are generally more reliable than *front/behind* judgments, and this asymmetry becomes stronger under sequential prompting. In Text-only mode at BS=1, all models already exhibit a positive left/right advantage, ranging from only a few points for Gemini to much larger gaps for Qwen and GPT-5.2. Under BS=20, this gap widens further for most models, indicating that depth-axis reasoning degrades faster than lateral reasoning as context accumulates. The same pattern appears in Scene Graph mode, where some models show even stronger imbalance between lateral and depth relations. In parallel, explicit inversion errors remain relatively uncommon in episodic evaluation but increase sharply under sequential load, especially for Kimi and the Qwen models. Taken together, these results suggest that long-context degradation does not simply reduce overall accuracy uniformly; instead, it disproportionately disrupts reasoning along the front/behind axis, while left/right relations remain comparatively more stable.

### 9.6 Top-View vs. Orbit-View Reasoning

Separating top-down questions from in-plane orbit transformations reveals a more nuanced picture of counterfactual spatial reasoning. In the episodic setting, top-view performance is strongly model-dependent: Gemini shows a pronounced top-view weakness relative to orbit-view averages, whereas several other models remain flatter or even improve on top-view questions under the same conditions. Under sequential evaluation, however, this pattern often reverses. As prompt depth increases, orbit-view performance deteriorates substantially faster than top-view performance, making top-down queries comparatively more robust for many model-representation pairs. This suggests that long-context interaction is especially destructive for maintaining rotated 3D egocentric relations, whereas flattened top-down reasoning can survive somewhat better once the underlying scene representation begins to degrade. In other words, severe sequential load appears to impair orbit-conditioned spatial state more than it impairs simpler allocentric projections, highlighting an important distinction between different forms of counterfactual viewpoint transformation.

### 9.7 Cross-Model Error Correlation and Shared Blind Spots

Beyond aggregate accuracy, cross-model error overlap reveals that failures are both shared and structured. Under lighter episodic settings, strong models often agree substantially, especially in Text-only mode, where pairs such as Gemini and GPT-5.2 frequently succeed on the same examples. Under heavier sequential settings, however, pairwise agreement becomes less informative on its own because models either fail together on a growing subset of questions or diverge into qualitatively different error modes. In particular, long-context Scene Graph evaluation produces both rising joint-failure rates and reduced agreement among otherwise strong models, indicating that stress induces heterogeneous collapse patterns rather than a single uniform degradation. At the same time, certain model families exhibit clear shared blind spots under load, with joint failure

Model	Arch	Params	Context	Max Out	Vision	Source	Peak input tokens	% Ctx
Gemini 3.1 Pro	Sparse MoE	Undisc.	1M	65K	Native MM	Closed	96,507	9.7%
GPT-5.2	Undisc.	Undisc.	400K	128K	Text+Image	Closed	41,205	10.3%
Qwen 3.5 Plus	DeltaNet+MoE	397B/17B	262K→1M	81K	Early fusion	Closed	86,772	33.1%
Qwen 3.5 OS	DeltaNet+MoE	397B/17B	262K→1M	81K	Early fusion	Open	86,772	33.1%
Kimi K2.5	MoE+MLA	1T/32B	262K	65K	MoonViT (400M)	Open	82,991	32.4%

**Table S3:** Architecture and resource profile of evaluated models, including maximum context window size, output limits, observed peak token consumption during CVT-Bench, and percentage of context consumed. GPT-5.2 uses batch size 10.

rates increasing markedly in BS=20 settings. Hard examples also cluster around recurring attributes, including top-view questions, some oblique rotations, dense scenes, and specific structured-input conditions. Consistent with this, the proportion of questions failed by all models rises substantially under long-context evaluation, especially in Image and Scene Graph modes. These findings reinforce the view that sequential spatial degradation is not merely a smooth drop in average F1, but a combination of increasing shared blind spots and model-specific instability.

## 10 Model/System Profile

### 10.1 Context and Token Utilization

Table S3 reports system-level characteristics and observed resource usage during evaluation, including maximum context length, maximum output constraints, vision integration type, and whether the model is open- or closed-source. Crucially, it also reports the peak token consumption observed during CVT-Bench runs and the corresponding fraction of the available context window used. These values contextualize sequential degradation results by showing that, even when prompts occupy a modest fraction of the context window (especially for long-context models), spatial accuracy and stability can still collapse. This supports the interpretation that the dominant failure mode is contextual interference and state instability rather than simple truncation or hard context overflow.

## 11 Reproducibility Details

### 11.1 Model Interfaces and API Settings

All models were evaluated using the provider-recommended default inference settings, and we did not tune decoding hyperparameters across models. Reasoning / thinking was enabled for all models when supported by the provider interface. Specifically, Gemini-3.1 Pro was queried through Google AI Studio, GPT-5.2 through the OpenAI API, Qwen-3.5 Plus and Qwen-3.5-397B-A17B through Alibaba DashScope, and Kimi-2.5 through OpenRouter. Unless otherwise noted, all unspecified parameters (e.g., temperature, top- $p$ , top- $k$ , and penalty terms) were left at provider defaults. Following the main paper, sequential experiments used batch size 20 for all models except GPT-5.2, which used batch size 10 due to output-length limitations under reasoning-enabled inference.

## 11.2 Prompt Templates for Each Representation

All three evaluation modes share the same overall structure: a *mode-specific context block* that defines the available scene representation and mode interpretation instructions, a *scene-specific context block* that describes the current scene corresponding to the mode, followed by a *shared question template* that instantiates spatial queries for the corresponding scene. The main methodological difference across modes is therefore the *input representation* rather than the wording of the downstream reasoning task. In Image mode, the model receives the rendered tagged image together with a scene-object dictionary. In Text-only mode, the image is replaced by a structured dictionary containing object descriptions and bounding boxes. In Scene Graph mode, the same dictionary is augmented with an explicit relational graph derived from the original ( $0^\circ$ ) viewpoint. To avoid redundancy, we present the three mode-specific master blocks separately below, followed by the shared question template used across all modes.

For sequential evaluation with batch size  $k > 1$ , the full prompt is constructed by concatenating  $k$  independent single-scene prompt instances in sequence after the mode-specific instructions, each consisting of its own scene-specific context block followed by its associated question block. In other words, the batch-size- $k$  prompt is a direct concatenation of the batch-size-1 template repeated  $k$  times, with no intermediate conversational turns or model-generated memory between scenes. This design preserves identical per-scene formatting across episodic and sequential settings while isolating the effect of context accumulation.

*Image mode.* In Image mode, the model is given the rendered CLEVR scene image with numeric tags overlaid on each object, along with a tag-to-description dictionary. This representation preserves the original visual input and evaluates multimodal spatial reasoning directly from pixels. The prompt first establishes the expected JSON output format, then presents the current image and its object dictionary, after which the shared question block is appended.

### Image-mode prompt

```
You will be given a series of images with questions about spatial
relationships between tagged objects. Answer all questions based
on careful spatial reasoning. Format your answers as a single JSON:
{"<image_name>": {"q_<id>": [relationships], ...}, ...}.
```

```
Input Image: CLEVR_new_000000.png
```

```
Refer to the numeric tags overlaid on the objects in the image.
```

```
Scene Object Dictionary: {"0": "small red metal cylinder", "1":
"small purple rubber cylinder", "2": "large brown metal cylinder",
"3": "small green rubber cube"}
```

```
[Shared question block appended here; see Question Template below.]
```

*Text-only mode (bounding boxes).* In Text-only mode, the image is removed and replaced with a structured textual scene description containing each tagged

object’s semantic description and bounding box coordinates  $[x, y, w, h]$ . This representation eliminates perception from the pipeline and isolates the model’s ability to reason over explicitly provided geometric structure. The output format is kept identical to Image mode, ensuring that differences in performance arise from representation changes rather than formatting changes.

### Text-only prompt

You will be given a series of scene descriptions with questions about spatial relationships between tagged objects. Answer all questions based on careful spatial reasoning. Format your answers as a single JSON: {"<image\_name>": {"q\_<id>": [relationships], ...}, ...}.

Input Image: CLEVR\_new\_000000.png

Refer to the bounding boxes  $[x, y, w, h]$  provided in the dictionary. Scene Object Dictionary: {"0": ("small red metal cylinder", [165, 71, 19, 25]), "1": ("small purple rubber cylinder", [81, 97, 24, 30]), "2": ("large brown metal cylinder", [174, 78, 49, 62]), "3": ("small green rubber cube", [130, 140, 25, 28])}

[Shared question block appended here; see Question Template below.]

*Scene Graph mode (text + bounding boxes + relations).* In Scene Graph mode, the textual object dictionary is further augmented with an explicit scene graph for the original ( $0^\circ$ ) view. This graph lists, for each tag, which other tags lie in each spatial direction. The model is instructed to use the object dictionary together with the scene graph for the anchor configuration and to mentally rotate the scene when answering counterfactual viewpoint queries. This representation provides the most explicit structural supervision and is intended to isolate whether failures arise from perception, from the lack of structured relational input, or from the reasoning process itself.

### Scene-graph prompt

You will be given a series of scenes. Each scene contains:

1. A Scene Object Dictionary: maps Tag IDs to object descriptions and bounding boxes  $[x, y, w, h]$ . No image is provided.
2. A Scene Graph for the original view ( $0^\circ$ ).

Format: ‘Tag X | dir:[A, B]’ means Tags A and B are in direction ‘dir’ relative to Tag X.

e.g. ‘Tag 0 | left:[1, 3]’ means Tag 1 and Tag 3 are to the LEFT of Tag 0.

Only directions with targets are listed; unlisted directions have no targets.

Answer all spatial relationship questions using the scene graph and object dictionary. For rotation questions, mentally rotate the scene from the original configuration. Format your answers as a single JSON: {"<image\_name>": {"q\_<id>": [relationships], ...}, ...}.

```

Scene 'CLEVR_new_000000.png':
Scene Object Dictionary: {"0": ("small red metal cylinder", [165, 71,
19, 25]), "1": ("small purple rubber cylinder", [81, 97, 24, 30]),
"2": ("large brown metal cylinder", [174, 78, 49, 62]), "3": ("small
green rubber cube", [130, 140, 25, 28])}
Scene Graph (original view):
Tag 0 | left:[1, 3] right:[2] front:[1, 2, 3]
Tag 1 | right:[0, 2, 3] front:[2, 3] behind:[0]
Tag 2 | left:[0, 1, 3] front:[3] behind:[0, 1]
Tag 3 | left:[1] right:[0, 2] behind:[0, 1, 2]

[Shared question block appended here; see Question Template below.]

```

*Shared question template.* After the mode-specific context block, all three representations use the same question-generation format. Counterfactual questions specify a target camera orbit angle  $\theta$  and a rotation direction (left or right), then ask for the new spatial relationship of one tagged object with respect to another. The answer space is multi-label, allowing multiple valid relations to be returned. For standard in-plane viewpoint transformations, the allowed predicates are [left, right, front, behind]. For top-down questions, the vertical-plane predicates are replaced by [north, south], yielding [left, right, north, south]. Thus, the task wording is held fixed across representations, while only the scene representation changes.

#### Shared question template

If the camera orbits <Theta> degrees to the <direction>, what is the new spatial relationship of the <object description> (Tag <object tag>) with respect to the <subject description> (Tag <subject tag>)? Choose from [left, right, front, behind]. Multiple relations possible.

For top-down questions, the same template is used with the answer choices changed to [left, right, north, south]:

#### Top-down variant

If the camera orbits to a top-down view, what is the new spatial relationship of the <object description> (Tag <object tag>) with respect to the <subject description> (Tag <subject tag>)? Choose from [left, right, north, south]. Multiple relations possible.